Available online at www.sciencedirect.com
ScienceDirect
Journal of Sound and Vibration 324 (2009) 798–815
JOURNAL OF SOUND AND VIBRATION
www.elsevier.com/locate/jsvi

Layer-wise modelling of magneto-electro-elastic plates

S.S. Phoenix[a,*], S.K. Satsangi[a], B.N. Singh[b]

[a]Department of Ocean Engineering and Naval Architecture, Indian Institute of Technology, Kharagpur 721 302, India
[b]Department of Aerospace Engineering, Indian Institute of Technology, Kharagpur 721 302, India

Received 6 May 2008; received in revised form 29 September 2008; accepted 22 February 2009
Handling Editor: L.G. Tham
Available online 24 March 2009

Abstract

This paper addresses the analysis of multi-layered plates with embedded/surface bonded piezoelectric/magnetostrictive layers using layer-wise mixed finite element method. The Reissner mixed variational theorem (RMVT) for composite/piezoelectric plates has been extended to the static and dynamic analysis of coupled magneto-electro-elastic problems. Transverse stress assumptions are made in the framework of RMVT and the resulting finite element describes a priori interlaminar continuous transverse shear and normal stresses. Numerical examples are solved to validate the present formulation using a code developed in C-language and the results obtained with the present model are in good agreement with the analytical solutions available in literature.

1. Introduction

Composite structures composed of piezoelectric and piezomagnetic materials possess the original piezoelectric and piezomagnetic properties along with a magneto-electric coupling effect that is not present in the constituents. Due to the ability of converting energy from one form to the other (among magnetic, electric, and mechanical energies), these materials have extensive applications in various sensors, actuators, hydrophones, medical ultrasonic imaging, etc.

Recent development of smart materials has stimulated considerable studies on the electric, magnetic, and mechanical behaviours of smart structures. A review of one-dimensional, two-dimensional, and three-dimensional approaches for the analysis of plates can be found in the articles by Saravanos et al. [1,2]. Recently, Pan [3], Guan and He [4], and Pan and Heyliger [5] presented exact solutions for the static analysis of simply supported, magneto-electro-elastic plates. Pan and Han [6] presented the exact solution for functionally graded anisotropic magneto-electro-elastic plate. Pan and Heyliger [7] also presented exact solution for the free-vibration analysis of simply supported, magneto-electro-elastic plates. Using state-space formulations, Chen et al. [8], Wang et al. [9], and Chen et al. [10] analysed magneto-electro-elastic plates whereas Chen and Lee [11] analysed functionally graded magneto-electro-elastic plates. Aimin et al. [12] made use of boundary contour method for the analysis of magneto-electro-elastic media. Bhangale and Ganesan

*Corresponding author. Tel.: +91 3222 281601; fax: +91 3222 255303.
E-mail addresses: phoenix@naval.iitkgp.ernet.in, febixss@yahoo.com (S.S. Phoenix).

0022-460X/$ - see front matter © 2009 Elsevier Ltd. All rights reserved.
doi:10.1016/j.jsv.2009.02.025

Nomenclature

a shorter length of the plate
b longer length of the plate
b (subscript) parameters related to layer bottom
$\mathbf{B} = [B_1, B_2, B_3]^T$ magnetic flux vector
$\mathbf{C}$ rigidity matrix of a lamina
d_{xy} magneto-electric coefficients
$\mathbf{D} = [D_1, D_2, D_3]^T$ electric displacement vector
e_{xy} piezoelectric constants
$\mathbf{E} = [E_1, E_2, E_3]^T$ electric field vector
$F_\tau = [F_t, F_b, F_r]^T$ functions of coefficients of Legendre polynomial
$\mathbf{g}$ nodal transverse stress vector
G (subscript) values calculated from geometrical relations
h thickness of the plate
h_k thickness of kth layer
$\mathbf{H} = [H_1, H_2, H_3]^T$ magnetic field vector
H (subscript) values calculated from Hooke's law
i, j (sub/superscript) number of node's expansions
k (sub/superscript) parameters related to kth layer
k_{xy} permittivity of material
$\mathbf{K}$ stiffness matrices
L_e work done due to external loads
M (subscript) values calculated from assumed model
$\mathbf{M}$ mass matrix
n (subscript) out-of-plane values
p (subscript) in-plane values
p_z amplitude of transverse applied pressure
$\mathbf{P}$ load vector
P_r coefficients of Legendre polynomial
$\mathbf{q}$ nodal displacement vector
q_{xy} magneto-electric constants
r (subscript) parameters related to intermediate sub-layers
t (subscript) parameters related to layer top
$\mathbf{u} = [u, v, w]^T$ displacement vector
V plate volume
x, y, z cartesian coordinate system
$\boldsymbol{\varepsilon} = [\varepsilon_{11}\ \varepsilon_{22}\ \varepsilon_{12}\ \varepsilon_{13}\ \varepsilon_{23}\ \varepsilon_{33}]^T$ strain vector
μ_{xy} permeability of material
ξ_k non-dimensional local layer coordinate
ρ density of the material
$\boldsymbol{\sigma} = [\sigma_{11}\ \sigma_{22}\ \sigma_{12}\ \sigma_{13}\ \sigma_{23}\ \sigma_{33}]^T$ stress vector
τ, s (sub/superscript) expansion of parameters along thickness direction
υ Poisson's ratio
$\boldsymbol{\Phi}$ nodal electric potential vector
$\boldsymbol{\psi}$ nodal magnetic potential vector
ω angular frequency
Ω plate reference surface

[13,14] presented static and free vibration analysis of functionally graded, anisotropic, and linear magneto-electro-elastic plates using semi-analytical finite element method. Few more relevant literature are also available in magneto-electric-elastic field particularly on the development of micro-mechanics model to evaluate the effective properties of a layered piezoelectric/piezomagnetic [15], extension of the potential theory method for the mixed boundary value problems [16], analysis of elliptical Hertzian contact [17], free vibration studies for Euler–Bernoulli beam [18] and approximate solution for the free vibration [19].

The applications of the Reissner mixed variational theorem (RMVT) for the analysis of multilayered composites can be found in the articles by Toledano [20] and Carrera [21–23]. A detailed review on the application of the Reissner mixed variational principle for composite plates can be seen in Ref. [24]. Formulation and numerical assessment of coupled multifield problems in piezoelectric structures can be found in the articles by Carrera et al. [25] and Carrera and Boscolo [26]. Carrera et al. [27] also presented variational statements and computational models for multifield problems. Benjeddou and Andrianarison [28], Ottavio and Kroplin [29], and Yang and Batra [30] presented mixed formulations for the laminated plates embedded with piezoelectric layers. Lage et al. [31] presented a partial mixed layer-wise finite element model based on the RMVT for static analysis of magneto-electro-elastic laminated plate structures.

In this paper, the RMVT as developed for composite/piezoelectric plates by Carrera and Demasi [32] has been extended to the static and dynamic analysis of coupled magneto-electro-elastic problems. A finite element model based on the RMVT for the analysis of magneto-electro-elastic plates is proposed and implemented which satisfies continuity of transverse stresses through the thickness direction. Mechanical displacements, electric potential, magnetic potential, and transverse stresses are considered as degrees of freedom. No post

processing procedure is required for the calculation of transverse stresses. The performance of the proposed mathematical formulation for static and forced vibration analysis of magneto-electro-elastic plates has been examined using computer code developed in C-language.

2. Finite element formulation

A multi-layered plate is a laminate obtained by stacking layers until the desired thickness and stiffness are obtained. Each lamina (piezoelectric, piezomagnetic or purely elastic) is considered homogeneous, perfectly bonded with each other and operating in the linear elastic range. The geometry and coordinate system used for the analysis of the laminated plate is shown in Fig. 1. $\xi_k = 2\ z_k/h_k$ is the non-dimensional local layer coordinate.

2.1. The RMVT for magneto-electro-elastic plates

This section discusses the derivation of the RMVT for magneto-electro-elastic plates. The energy function for a magneto-electro-elastic continuum can be written as the sum of mechanical, electric, and magnetic energy.

$$G = \tfrac{1}{2}\boldsymbol{\varepsilon}^{\mathrm{T}}\mathbf{C}\boldsymbol{\varepsilon} - \tfrac{1}{2}\mathbf{E}^{\mathrm{T}}\mathbf{k}\mathbf{E} - \tfrac{1}{2}\mathbf{H}^{\mathrm{T}}\boldsymbol{\mu}\mathbf{H} - \mathbf{E}^{\mathrm{T}}\mathbf{e}\boldsymbol{\varepsilon} - \mathbf{H}^{\mathrm{T}}\mathbf{q}\boldsymbol{\varepsilon} - \mathbf{H}^{\mathrm{T}}\,\mathbf{d}\mathbf{E} \tag{1}$$

Differentiation of the energy function as given in Eq. (1) with respect to strain electric field and magnetic field gives the stress vector, electric, and magnetic displacement vectors which are expressed as

$$\boldsymbol{\sigma} = \frac{\partial G}{\partial \boldsymbol{\varepsilon}}; \quad \mathbf{D} = -\frac{\partial G}{\partial \mathbf{E}}; \quad \mathbf{B} = -\frac{\partial G}{\partial \mathbf{H}} \tag{2}$$

The constitutive equations are therefore obtained as

$$\boldsymbol{\sigma} = \mathbf{C}\boldsymbol{\varepsilon} - \mathbf{e}\mathbf{E} - \mathbf{q}\mathbf{H}; \quad \mathbf{D} = \mathbf{e}^{\mathbf{T}}\boldsymbol{\varepsilon} + \mathbf{k}\mathbf{E} + \mathbf{d}\mathbf{H}; \quad \mathbf{B} = \mathbf{q}^{\mathbf{T}}\boldsymbol{\varepsilon} + \boldsymbol{\mu}\mathbf{H} + \mathbf{d}\mathbf{E} \tag{3}$$

For the sake of convenience from computational point of view, the stresses and strains are broken into in-plane and out-of-plane components as

$$\boldsymbol{\sigma}_p = [\sigma_{11}\ \ \sigma_{22}\ \ \sigma_{12}]^{\mathrm{T}}; \quad \boldsymbol{\sigma}_n = [\sigma_{13}\ \ \sigma_{23}\ \ \sigma_{33}]^{\mathrm{T}} \tag{4}$$

$$\boldsymbol{\varepsilon}_p = [\varepsilon_{11}\ \ \varepsilon_{22}\ \ \varepsilon_{12}]^{\mathrm{T}}; \quad \boldsymbol{\varepsilon}_n = [\varepsilon_{13}\ \ \varepsilon_{23}\ \ \varepsilon_{33}]^{\mathrm{T}} \tag{5}$$

Hence, the constitutive equations for a magneto-electro-elastic material can be written as

$$\boldsymbol{\sigma}_n = \mathbf{c}_{pn}^{\mathrm{T}}\boldsymbol{\varepsilon}_p + \mathbf{c}_{nn}\boldsymbol{\varepsilon}_n - \mathbf{e}_n\mathbf{E} - \mathbf{q}_n\mathbf{H}; \quad \boldsymbol{\sigma}_p = \mathbf{c}_{pp}\boldsymbol{\varepsilon}_p + \mathbf{c}_{pn}\boldsymbol{\varepsilon}_n - \mathbf{e}_p\mathbf{E} - \mathbf{q}_p\mathbf{H} \tag{6}$$

$$\mathbf{D} = \mathbf{e}_p^{\mathrm{T}}\boldsymbol{\varepsilon}_p + \mathbf{e}_n\boldsymbol{\varepsilon}_n + \mathbf{k}\mathbf{E} + \mathbf{d}\mathbf{H}; \quad \mathbf{B} = \mathbf{q}_p^{\mathrm{T}}\boldsymbol{\varepsilon}_p + \mathbf{q}_n\boldsymbol{\varepsilon}_n + \boldsymbol{\mu}\mathbf{H} + \mathbf{d}\mathbf{E} \tag{7}$$

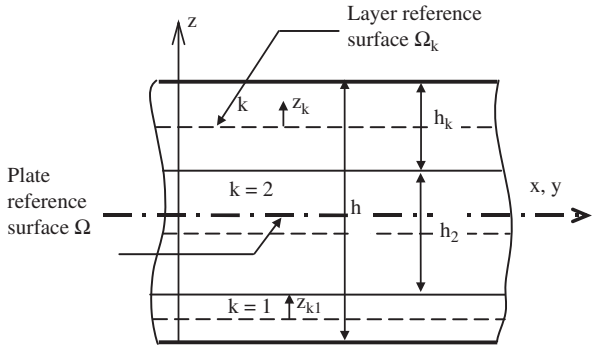

Fig. 1. Geometry and coordinate system of laminated plates.

The explicit form of the introduced matrices in Eqs. (6) and (7) is as follows:

$$\mathbf{c}_{pp}=\begin{bmatrix} c_{11} & c_{12} & c_{16} \\ c_{12} & c_{22} & c_{26} \\ c_{16} & c_{26} & c_{66} \end{bmatrix};\quad \mathbf{c}_{nn}=\begin{bmatrix} c_{55} & c_{45} & 0 \\ c_{45} & c_{44} & 0 \\ 0 & 0 & c_{33} \end{bmatrix};\quad \mathbf{c}_{pn}=\begin{bmatrix} 0 & 0 & c_{13} \\ 0 & 0 & c_{23} \\ 0 & 0 & c_{36} \end{bmatrix}=\mathbf{c}_{np}^{\mathrm{T}} \tag{8}$$

$$\mathbf{e}_{p}=\begin{bmatrix} 0 & 0 & e_{31} \\ 0 & 0 & e_{32} \\ 0 & 0 & e_{36} \end{bmatrix};\quad \mathbf{e}_{n}=\begin{bmatrix} e_{15} & e_{25} & 0 \\ e_{14} & e_{24} & 0 \\ 0 & 0 & e_{33} \end{bmatrix};\quad \mathbf{k}=\begin{bmatrix} k_{11} & k_{12} & 0 \\ k_{12} & k_{22} & 0 \\ 0 & 0 & k_{33} \end{bmatrix} \tag{9}$$

$$\boldsymbol{\mu}=\begin{bmatrix} \mu_{11} & \mu_{12} & 0 \\ \mu_{12} & \mu_{22} & 0 \\ 0 & 0 & \mu_{33} \end{bmatrix};\quad \mathbf{d}=\begin{bmatrix} d_{11} & d_{12} & 0 \\ d_{12} & d_{22} & 0 \\ 0 & 0 & d_{33} \end{bmatrix};\quad \mathbf{q}_{p}=\begin{bmatrix} 0 & 0 & q_{31} \\ 0 & 0 & q_{32} \\ 0 & 0 & q_{36} \end{bmatrix} \tag{10}$$

$$\mathbf{q}_{n}=\begin{bmatrix} q_{15} & q_{25} & 0 \\ q_{14} & q_{24} & 0 \\ 0 & 0 & q_{33} \end{bmatrix};\quad \mathbf{E}^{\mathrm{T}}=[E_1\ \ E_2\ \ E_3];\quad \mathbf{D}^{\mathrm{T}}=[D_1\ \ D_2\ \ D_3] \tag{11}$$

$$\mathbf{B}^{\mathrm{T}}=[B_1\ \ B_2\ \ B_3];\quad \mathbf{H}^{\mathrm{T}}=[H_1\ \ H_2\ \ H_3];\quad \mathbf{u}_{\tau i}^{k\mathrm{T}}=[u\ \ v\ \ w] \tag{12}$$

The strain–displacement relationship is

$$\boldsymbol{\varepsilon}_{pG}=\mathbf{D}_{p}\mathbf{u};\quad \boldsymbol{\varepsilon}_{nG}=\mathbf{D}_{n}\mathbf{u}=(\mathbf{D}_{n\Omega}+\mathbf{D}_{nz})\mathbf{u} \tag{13}$$

The differential matrices are

$$\mathbf{D}_{p}=\begin{bmatrix} \dfrac{\partial}{\partial x} & 0 & 0 \\ 0 & \dfrac{\partial}{\partial y} & 0 \\ \dfrac{\partial}{\partial y} & \dfrac{\partial}{\partial x} & 0 \end{bmatrix};\quad \mathbf{D}_{nz}=\begin{bmatrix} \dfrac{\partial}{\partial z} & 0 & 0 \\ 0 & \dfrac{\partial}{\partial z} & 0 \\ 0 & 0 & \dfrac{\partial}{\partial z} \end{bmatrix};\quad \mathbf{D}_{n\Omega}=\begin{bmatrix} 0 & 0 & \dfrac{\partial}{\partial x} \\ 0 & 0 & \dfrac{\partial}{\partial y} \\ 0 & 0 & 0 \end{bmatrix} \tag{14}$$

$$\mathbf{E}^{\mathrm{T}}=[-\partial x\ \ -\partial y\ \ -\partial z]\boldsymbol{\Phi};\quad \mathbf{H}^{\mathrm{T}}=[-\partial x\ \ -\partial y\ \ -\partial z]\boldsymbol{\psi} \tag{15}$$

$$\mathbf{E}=(D_{ep}+D_{ez})\boldsymbol{\Phi};\quad \mathbf{H}=(D_{ep}+D_{ez})\boldsymbol{\psi};\quad D_{ep}^{\mathrm{T}}=[-\partial x\ \ -\partial y\ \ 0];\quad D_{ez}^{\mathrm{T}}=[0\ \ 0\ \ -\partial z] \tag{16}$$

The variation of potential energy for a magneto-electro-elastic continuum can be written as the sum of variation of mechanical energy, electric energy, magnetic energy and the variation of work done by applied loadings. An extension of the RMVT to magneto-electro-elastic material is presented in this section. Since the transverse stresses are also taken as nodal degrees of freedom in the mixed theories $\boldsymbol{\sigma}_{nM}$ should be introduced into the PVD equations.

The potential energy of a system can be expressed as

$$\begin{aligned}\delta L-\delta U&=\delta\int_{V}[G(\boldsymbol{\varepsilon}_{pG},\boldsymbol{\varepsilon}_{nG},\mathbf{E},\mathbf{H})+\boldsymbol{\sigma}_{nM}(\boldsymbol{\varepsilon}_{nG}-\boldsymbol{\varepsilon}_{nH})]\,\mathrm{d}V\\&=\int_{V}\left[\delta\boldsymbol{\varepsilon}_{pG}^{\mathrm{T}}\frac{\partial G}{\partial\boldsymbol{\varepsilon}_{pG}}+\delta\boldsymbol{\varepsilon}_{nG}^{\mathrm{T}}\frac{\partial G}{\partial\boldsymbol{\varepsilon}_{nG}}+\delta\mathbf{E}^{\mathrm{T}}\frac{\partial G}{\partial E}+\delta\mathbf{H}^{\mathrm{T}}\frac{\partial G}{\partial H}+\delta\boldsymbol{\sigma}_{nM}^{\mathrm{T}}(\boldsymbol{\varepsilon}_{nG}-\boldsymbol{\varepsilon}_{nH})\right]\mathrm{d}V\\&=\sum_{k=1}^{N_l}\int_{A_k}\int_{\Omega_k}[\delta\boldsymbol{\varepsilon}_{pG}^{kT}\boldsymbol{\sigma}_{pH}^{k}+\delta\boldsymbol{\varepsilon}_{nG}^{kT}\boldsymbol{\sigma}_{nM}^{k}-\delta\mathbf{E}^{kT}\mathbf{D}^{k}-\delta\mathbf{H}^{kT}\mathbf{B}^{k}+\delta\boldsymbol{\sigma}_{nM}^{\mathrm{T}}(\varepsilon_{nG}-\varepsilon_{nH})]\,\mathrm{d}\Omega_k\,\mathrm{d}z\end{aligned} \tag{17}$$

where subscripts G, H, and M denote values calculated from geometrical relations, Hooke's law, and assumed model, respectively. The left hand side terms of Eq. (17) are expressed as

$$\delta U = \sum_{k=1}^{N_l} \int_V (\rho_k \delta u^{\mathrm{T}} \ddot{\mathbf{u}})\, \mathrm{d}V \tag{18}$$

$$\delta L = \delta L_{el} + \delta L_e + \delta L_m \tag{19}$$

here the work done due to the applied surface charge, L_e and work done due to the applied surface magnetic charges, L_m are taken as zeroes, and L_{el} is the work done due to external load of intensity p_z.

The constitutive equations for $\boldsymbol{\sigma}_{pH}$, $\boldsymbol{\varepsilon}_{nH}$, $\mathbf{D}$, and $\mathbf{B}$ can be directly obtained by taking out $\boldsymbol{\varepsilon}_n$ from Eq. (6) and substituting in Eq. (7). The resulting constitutive equations are rearranged and are given below:

$$\boldsymbol{\sigma}_{pH} = \bar{\mathbf{c}}_{pp}\boldsymbol{\varepsilon}_{pG} + \bar{\mathbf{c}}_{pn}\boldsymbol{\sigma}_{nM} + \bar{\mathbf{c}}_{se}\mathbf{E} + \bar{\mathbf{c}}_{sq}\mathbf{H}; \quad \boldsymbol{\varepsilon}_{nH} = \bar{\mathbf{c}}_{np}\boldsymbol{\varepsilon}_{pG} + \bar{\mathbf{c}}_{nn}\boldsymbol{\sigma}_{nM} + \bar{\mathbf{c}}_{de}\mathbf{E} + \bar{\mathbf{c}}_{dq}\mathbf{H} \tag{20}$$

$$\mathbf{D} = \bar{\mathbf{c}}_{ed}\boldsymbol{\varepsilon}_{pG} + \bar{\mathbf{c}}_{es}\boldsymbol{\sigma}_{nM} + \bar{\mathbf{c}}_{ee}\mathbf{E} + \bar{\mathbf{c}}_{eq}\mathbf{H}; \quad \mathbf{B} = \bar{\mathbf{c}}_{qd}\boldsymbol{\varepsilon}_{pG} + \bar{\mathbf{c}}_{qs}\boldsymbol{\sigma}_{nM} + \bar{\mathbf{c}}_{qe}\mathbf{E} + \bar{\mathbf{c}}_{qq}\mathbf{H} \tag{21}$$

where

$$\bar{\mathbf{c}}_{pp} = \mathbf{c}_{pp} - \mathbf{c}_{pn}\mathbf{c}_{nn}^{-1}\mathbf{c}_{np}; \quad \bar{\mathbf{c}}_{pn} = \mathbf{c}_{pn}\mathbf{c}_{nn}^{-1}; \quad \bar{\mathbf{c}}_{se} = \mathbf{c}_{pn}\mathbf{c}_{nn}^{-1}\mathbf{e}_n - \mathbf{e}_p; \quad \bar{\mathbf{c}}_{sq} = \mathbf{c}_{pn}\mathbf{c}_{nn}^{-1}\mathbf{q}_n - \mathbf{q}_p$$

$$\bar{\mathbf{c}}_{np} = -\mathbf{c}_{nn}^{-1}\mathbf{c}_{np}; \quad \bar{\mathbf{c}}_{nn} = \mathbf{c}_{nn}^{-1}; \quad \bar{\mathbf{c}}_{de} = -\mathbf{c}_{nn}^{-1}\mathbf{e}_n; \quad \bar{\mathbf{c}}_{dq} = \mathbf{c}_{nn}^{-1}\mathbf{q}_n; \quad \bar{\mathbf{c}}_{ed} = \mathbf{e}_p^{\mathrm{T}} - \mathbf{e}_n^{\mathrm{T}}\mathbf{c}_{nn}^{-1}\mathbf{c}_{np}$$

$$\bar{\mathbf{c}}_{es} = \mathbf{e}_n^{\mathrm{T}}\mathbf{c}_{nn}^{-1}; \quad \bar{\mathbf{c}}_{qd} = \mathbf{q}_p^{\mathrm{T}} - \mathbf{q}_n^{\mathrm{T}}\mathbf{c}_{nn}^{-1}\mathbf{c}_{np}; \quad \bar{\mathbf{c}}_{qs} = \mathbf{q}_n^{\mathrm{T}}\mathbf{c}_{nn}^{-1}; \quad \bar{\mathbf{c}}_{ee} = \mathbf{e}_n^{\mathrm{T}}\mathbf{c}_{nn}^{-1}\mathbf{e}_n + \mathbf{k}$$

$$\bar{\mathbf{c}}_{eq} = \mathbf{e}_n^{\mathrm{T}}\mathbf{c}_{nn}^{-1}\mathbf{q}_n + \mathbf{d}; \quad \bar{\mathbf{c}}_{qq} = \mathbf{q}_n^{\mathrm{T}}\mathbf{c}_{nn}^{-1}\mathbf{q}_n + \boldsymbol{\mu}; \quad \bar{\mathbf{c}}_{qe} = \mathbf{q}_n^{\mathrm{T}}\mathbf{c}_{nn}^{-1}\mathbf{e}_n + \mathbf{d}$$

In the present model each layer is considered as independent layer and continuity of field variables are imposed as constraints. For Taylor type expansions of field variables along the thickness requires additional conditions for satisfying top and bottom continuity. Hence combinations of legendry polynomials are used for the expansion of field variables through thickness direction. The displacement, transverse stress, electric, and magnetic fields along thickness direction are assumed as follows:

$$\left.\begin{aligned} \mathbf{u}^k &= F_t u_t + F_b u_b + F_r u_r = F_\tau u_\tau = F_\tau N_i q_{\tau i} \\ \boldsymbol{\sigma}_{nM}^k &= F_t \sigma_{nt}^k + F_b \sigma_{nb}^k + F_r \sigma_{nr}^k = F_\tau \sigma_\tau = F_\tau N_i g_{\tau i} \\ \boldsymbol{\phi}^k &= F_t \phi_t + F_b \phi_b + F_r \phi_r = F_\tau \phi_\tau = F_\tau N_i \phi_{\tau i} \\ \psi^k &= F_t \psi_t + F_b \psi_b + F_r \psi_r = F_\tau \psi_\tau = F_\tau N_i \psi_{\tau i}; \\ \tau &= t, b, r \quad \text{and} \quad i = 0, 1, \ldots, N \end{aligned}\right\} \tag{22}$$

where N is the number of nodes per element, N_i the shape function for the eight-noded isoparametric element, and

$$F_b = \frac{(P_0 + P_1)}{2} = \frac{(1 + \xi_k)}{2}; \quad F_t = \frac{(P_0 - P_1)}{2} = \frac{(1 - \xi_k)}{2}; \quad \text{and} \quad F_r = (P_r - P_{r-2}) \tag{23}$$

The number of sub-layers in each layer is taken as one number higher than the order of variation of the degrees of freedom considered. Hence 'r' in the function F_r will take values from 2 onwards according to the number of sub-layers. The function P_r is the respective coefficient of Legendre polynomial. In the present formulation, order of polynomials along thickness direction can be varied independently. For example, if the order of variation of degrees of freedom along thickness direction is taken as 4 there will be 5 sub-layers in each layer and 'r' in the function F_r will take values 2, 3, 4 and $F_b = F_1$; $F_t = F_5$.

The function chosen have the following properties:

$$\xi_k = \begin{cases} 1; & F_t = 1, \quad F_b = 0, \quad F_r = 0 \\ -1; & F_t = 0, \quad F_b = 1, \quad F_r = 0 \end{cases} \tag{24}$$

It may be noted that the layer-wise description does not require any zig-zag function for the simulation of zig-zag effects. The continuity of the displacement at each interface can be linked using Eq. (25).

$$u_t^k = u_b^{(k+1)}, \quad k = 1, \quad N_l - 1 \quad \text{and} \quad \boldsymbol{\sigma}_{nt}^k = \boldsymbol{\sigma}_{nb}^{k+1} \tag{25}$$

On substitution of Eqs. (16), (18), (23), (24), (25) in Eq. (20), one gets Eq. (26) (similar formulation for composite plates can be found in Carrera and Demasi [32]).

$$\begin{aligned}\delta L - \delta U = {} & \delta \mathbf{q}^{kT}(\mathbf{K}_{uu}^{k\tau sij}\mathbf{q}^k + \mathbf{K}_{u\sigma}^{k\tau sij}\mathbf{g}^k + \mathbf{K}_{ue}^{k\tau sij}\boldsymbol{\phi}^k + \mathbf{K}_{uq}^{k\tau sij}\boldsymbol{\psi}^k) \\ & + \delta \mathbf{g}^{kT}(\mathbf{K}_{\sigma u}^{k\tau sij}\mathbf{q}^k + \mathbf{K}_{\sigma\sigma}^{k\tau sij}\mathbf{g}^k + \mathbf{K}_{\sigma e}^{k\tau sij}\boldsymbol{\phi}^k + \mathbf{K}_{\sigma q}^{k\tau sij}\boldsymbol{\psi}^k) \\ & + \delta \boldsymbol{\phi}^{kT}(\mathbf{K}_{eu}^{k\tau sij}\mathbf{q}^k + \mathbf{K}_{e\sigma}^{k\tau sij}\mathbf{g}^k + \mathbf{K}_{ee}^{k\tau sij}\boldsymbol{\phi}^k + \mathbf{K}_{eq}^{k\tau sij}\boldsymbol{\psi}^k) \\ & + \delta \boldsymbol{\psi}^{kT}(\mathbf{K}_{qu}^{k\tau sij}\mathbf{q}^k + \mathbf{K}_{q\sigma}^{k\tau sij}\mathbf{g}^k + \mathbf{K}_{qe}^{k\tau sij}\boldsymbol{\phi}^k + \mathbf{K}_{qq}^{k\tau sij}\boldsymbol{\psi}^k)\end{aligned} \tag{26}$$

The equilibrium and compatibility equations obtained from the above equation for a magneto-electro-elastic material are given below:

$$\mathbf{K}_{uu}^{k\tau sij}\mathbf{q}^k + \mathbf{K}_{u\sigma}^{k\tau sij}\mathbf{g}^k + \mathbf{K}_{ue}^{k\tau sij}\boldsymbol{\phi}^k + \mathbf{K}_{uq}^{k\tau sij}\boldsymbol{\psi}^k = \mathbf{p}^k \tag{27}$$

$$\mathbf{K}_{\sigma u}^{k\tau sij}\mathbf{q}^k + \mathbf{K}_{\sigma\sigma}^{k\tau sij}\mathbf{g}^k + \mathbf{K}_{\sigma e}^{k\tau sij}\boldsymbol{\phi}^k + \mathbf{K}_{\sigma q}^{k\tau sij}\boldsymbol{\psi}^k = 0 \tag{28}$$

$$\mathbf{K}_{eu}^{k\tau sij}\mathbf{q}^k + \mathbf{K}_{e\sigma}^{k\tau sij}\mathbf{g}^k + \mathbf{K}_{ee}^{k\tau sij}\boldsymbol{\phi}^k + \mathbf{K}_{eq}^{k\tau sij}\boldsymbol{\psi}^k = 0 \tag{29}$$

$$\mathbf{K}_{qu}^{k\tau sij}\mathbf{q}^k + \mathbf{K}_{q\sigma}^{k\tau sij}\mathbf{g}^k + \mathbf{K}_{qe}^{k\tau sij}\boldsymbol{\phi}^k + \mathbf{K}_{qq}^{k\tau sij}\boldsymbol{\psi}^k = 0 \tag{30}$$

where $\mathbf{K}_{\sigma u}^{k\tau sij}, \mathbf{K}_{\sigma\sigma}^{k\tau sij}, \mathbf{K}_{\sigma e}^{k\tau sij}, \mathbf{K}_{\sigma q}^{k\tau sij}\mathbf{K}_{uu}^{k\tau sij}, \mathbf{K}_{ue}^{k\tau sij}, \mathbf{K}_{uq}^{k\tau sij}$, etc. are the stiffness matrices arising due to coupled and uncoupled terms of magneto-elastic-electro material and the same are provided in Appendix A.

In the present analysis an eight-noded isoparametric plate element is used for the finite element discretization. Each lamina in a laminate is divided into a number of sub-layers according to the order of variations of displacement and transverse stress fields across thickness. The degrees of freedom corresponding to transverse stress parameters are eliminated at element level. Stiffness matrices are calculated separately for each sub-layer combination. Each sub-layer has its own unique value of the stiffness matrices depending upon their interpolation function values along the thickness direction. After obtaining the stiffness matrix, $\mathbf{K}_{\text{mixed}}$ and mass matrix $\mathbf{M}$ for an element extended over the full thickness of the plate it has to be assembled along the in-plane direction to form the overall stiffness matrix and mass matrix of the whole system. Then the governing equation for dynamic response is solved by direct time integration scheme following Newmark's β method [33].

3. Numerical examples

A number of examples are solved in this section to study the static and transient vibration behaviour of linear magneto-electro-elastic laminates. In all the cases the magnetic and the electric potentials at the boundaries are assumed as zero. First, a three-layered sandwich magneto-electro-elastic plate with known analytical solution [3] is examined in order to validate the mixed finite element model code based on the RMVT which has been presented in the previous section. Analysis of a three-layered sandwich magneto-electro-elastic plate under different types of loadings is considered in the first example. In the second example, a two-layer magneto-electro-elastic plate made of $BaTiO_3/CoFe_2O_4$ is studied under different span to depth ratios and boundary conditions. To the best of the authors' knowledge, the results are not readily available in the literature for transient analysis of magneto-electro-elastic plates. Hence the present example results are validated for piezoelectric plate with that of Ray et al. [34]. In the third example forced vibration analysis of a three-layer simply supported plate having different span to depth ratios is presented along with the convergence study results. As a final example, dynamic transient analysis of a sandwich smart plate is

presented. The various quantities used in tables and figures are as follows:

$$(u^*, v^*) = (u, v)/(a/h)^3, \quad w^* = w100/(a/h)^4, \quad (D_x^*, D_y^*, B_x^*, B_y^*) = (D_x, D_y, B_x, B_y)/(a/h)$$

$$(\sigma_{xx}^*, \sigma_{yy}^*, \sigma_{xy}^*, \Phi^*, \psi^*) = (\sigma_{xx}, \sigma_{yy}, \sigma_{xy}, \Phi, \psi)/(a/h)^2, \quad (\sigma_{zx}^*, \sigma_{zy}^*) = (\sigma_{xx}, \sigma_{yy})/(a/h)$$

The following material properties are used for the computation of the results unless mentioned otherwise:

	$c_{11} = c_{22}$	c_{33}	c_{12}	$c_{13} = c_{23}$	$c_{44} = c_{55}$	$c_{66} = (c_{11} - c_{12})0.5$	
$BaTiO_3$	166	162	77	78	43	44.5	
$CoFe_2O_4$	286	173	170.5	269.5	45.3	56.5	
	$e_{13} = e_{23}$	e_{33}	$e_{24} = e_{15}$	$k_{11} = k_{22}$	k_{33}	$\mu_{11} = \mu_{22}$	μ_{33}
$BaTiO_3$	−4.4	18.6	11.6	11.2	12.6	5	10
	$q_{13} = q_{23}$	q_{33}	$q_{24} = q_{15}$	$k_{11} = k_{22}$	k_{33}	$\mu_{11} = \mu_{22}$	μ_{33}
$CoFe_2O_4$	580.3	699.7	550	0.08	0.093	−590	157

The units of material properties given above are: c_{ij} in GPa, q_{ij} in N/(Am), e_{ij} in C/m^2, k_{ij} in 10^{-9} C^2/(Nm^2), and μ_{ij} in 10^{-6} Ns^2/C^2.

3.1. Static analysis

3.1.1. Example-1

In this example sandwich plate made of piezoelectric $BaTiO_3$ and magnetostrictive $CoFe_2O_4$ as reported in Pan [3] is analysed for the validation of the present finite element based RMVT model. The thickness (h) of the plate having three layers of equal thickness is given as 0.3 m. The simply supported boundary conditions and bi-sinusoidal loading ($p = \sin(\pi x/a)\sin(\pi y/b)$ where a and b are shorter and longer dimensions of the plate at the top surface of the plate are considered [3]. Two different stacking sequences namely ($BaTiO_3/CoFe_2O_4/BaTiO_3$ (B/F/B) and $CoFe_2O_4/BaTiO_3/CoFe_2O_4$ (F/B/F)) are taken. The values of electric and magnetic potentials at coordinates $x = 0.75$, $y = 0.25$ with the analytical solution of Pan [3] are tabulated in Table 1 for different mesh sizes. From the table it is observed that the results converge very well and the results with 4×4 mesh size show good convergence and accuracy. It is also observed that the present results are in good agreement with that of Pan [3].

Table 1
Convergence and validation study for φ and $\mathbf{\Psi}$ at $x = 0.75$, $y = 0.25$.

	B/F/B		F/B/F	
	$\mathbf{\Phi}$	Ψ	$\mathbf{\Phi}$	Ψ
Present				
4×4				
$z = 0.00$	8.010×10^{-4}	-2.515×10^{-6}	1.895×10^{-3}	-1.181×10^{-6}
$z = 0.15$	1.355×10^{-3}	-2.570×10^{-6}	2.292×10^{-3}	-1.670×10^{-6}
$z = 0.30$	1.043×10^{-3}	-2.180×10^{-6}	2.144×10^{-3}	-8.648×10^{-6}
8×8				
$z = 0.00$	8.007×10^{-4}	-2.517×10^{-6}	1.897×10^{-3}	-1.182×10^{-6}
$z = 0.15$	1.358×10^{-3}	-2.570×10^{-6}	2.293×10^{-3}	-1.670×10^{-6}
$z = 0.30$	1.049×10^{-3}	-2.181×10^{-6}	2.147×10^{-3}	-8.650×10^{-6}
12×12				
$z = 0.00$	8.006×10^{-4}	-2.520×10^{-6}	1.897×10^{-3}	-1.184×10^{-6}
$z = 0.15$	1.358×10^{-3}	-2.570×10^{-6}	2.294×10^{-3}	-1.670×10^{-6}
$z = 0.30$	1.050×10^{-3}	-2.183×10^{-6}	2.148×10^{-3}	-8.653×10^{-6}
Pan [3]				
$z = 0.00$	7.874×10^{-4}	-2.527×10^{-6}	1.900×10^{-3}	-1.246×10^{-6}
$z = 0.15$	1.359×10^{-3}	-2.600×10^{-6}	2.297×10^{-3}	-1.670×10^{-6}
$z = 0.30$	1.053×10^{-3}	-2.188×10^{-6}	2.154×10^{-3}	-8.692×10^{-6}

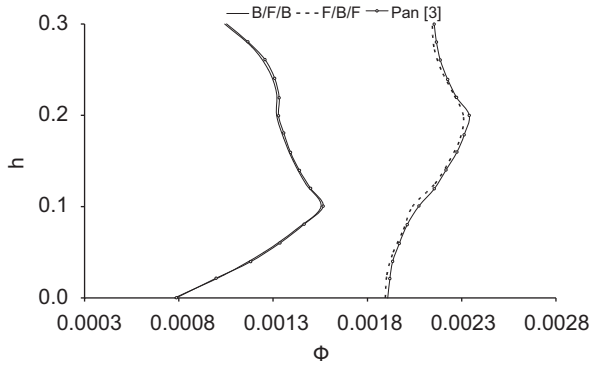

Fig. 2. Variation of $\mathbf{\Phi}$ across the thickness under bi-sinusoidal loading.

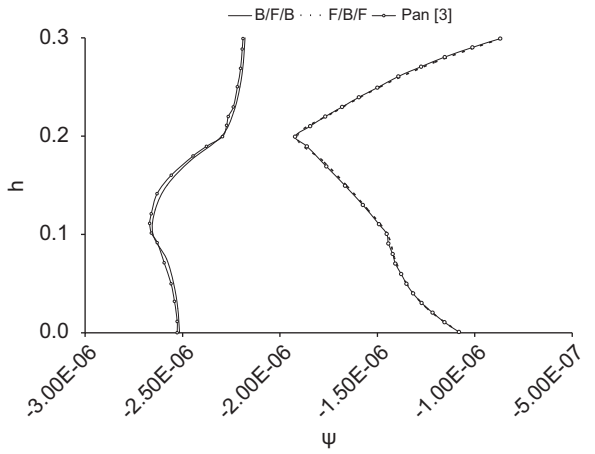

Fig. 3. Variation of ψ across the thickness under bi-sinusoidal loading.

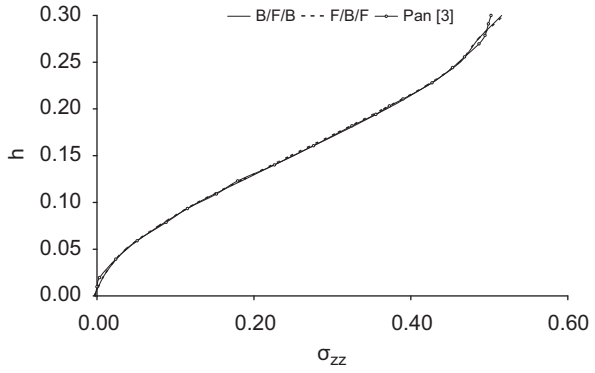

Fig. 4. Variation of σ_{zz} across the thickness under bi-sinusoidal loading.

In another validation study, the variations of Φ, ψ, σ_{zz}, D_x, and B_x across the thickness under bi-sinusoidal loading along with the results of Pan [3] are plotted in Figs. 2–6. It can be seen from the figures that the cross-thickness distributions (evaluated at coordinates $x = 0.75$, $y = 0.25$) for primary and secondary variables are in good agreement with those of Pan [3]. The variation of electric and magnetic potentials shown in Figs. 2 and 3 are found to be continuous at layer interfaces but their slopes are discontinuous. Normal stress across the thickness as shown in the Fig. 4 has a continuous positive slope throughout the thickness. It can also be seen

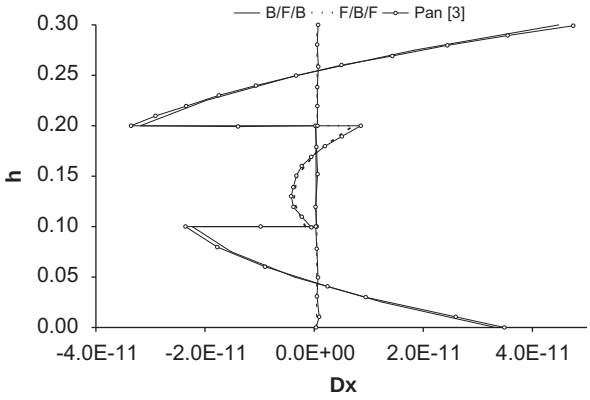

Fig. 5. Variation of D_x across the thickness under bi-sinusoidal loading.

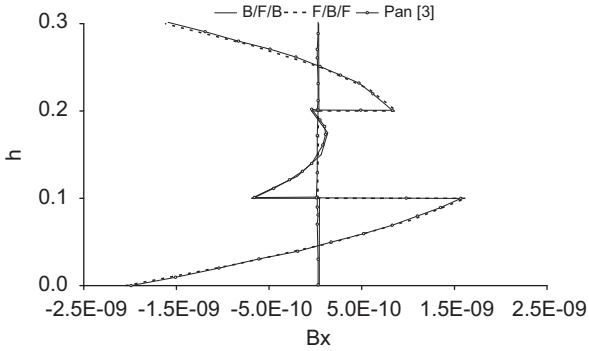

Fig. 6. Variation of B_x across the thickness under bi-sinusoidal loading.

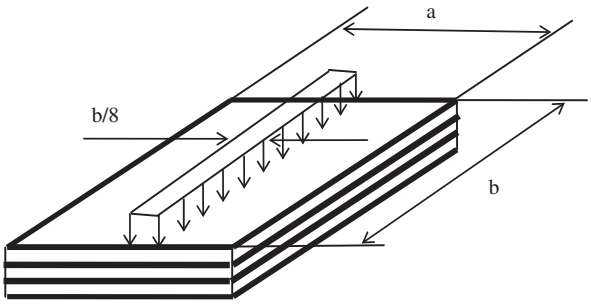

Fig. 7. Plate subjected to localized uniformly distributed load at the centre.

from the Fig. 4 that the stacking sequence (F/B/F or B/F/B) has not much influence in the variation pattern of normal stresses except at the top layer, where it shows a slight difference in nature of slope. Fig. 5 shows that the electric displacement varies drastically across the $BaTiO_3$ layer, whereas its value is more or less zero in $CoFe_2O_4$. Similarly, in Fig. 6 the magnetic displacement varies drastically across the $CoFe_2O_4$ layer, whereas its value is more or less than zero in $BaTiO_3$.

Some new results are presented for this example. As defined earlier, a simply supported sandwich plate made of piezoelectric $BaTiO_3$ and magnetostrictive $CoFe_2O_4$ is analysed. The plate has three layers of equal thickness $h = 0.3$ m. Two different stacking sequences considered are B/F/B and F/B/F. The plate is analysed with two different types of loadings namely uniformly distributed load ($p = 3\,\mathrm{N/m^2}$) and a bi-sinusoidal potential applied at the top surface of the plate as shown in Figs. 7 and 8, respectively. The results for u, v, w, Φ, ψ, σ, D, and B evaluated at coordinates ($x = 0.75$, $y = 0.25$, $z = 0.0$) for the plate under external potential

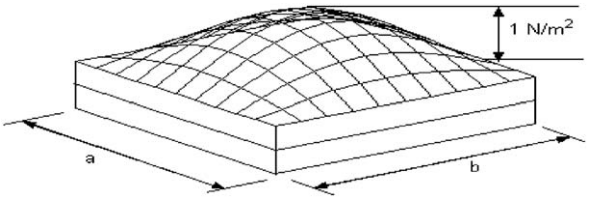

Fig. 8. Plate subjected to bi-sinusoidal loading for F/B plate.

Table 2
Results for simply supported plate for applied potential and line loading.

	Potential loading		Line loading	
	B/F/B	F/B/F	B/F/B	F/B/F
$u*10^{13}$	−248.26	−4.2094	21.408	16.505
$v*10^{13}$	248.26	4.2094	−17.772	−13.902
$w*10^{12}$	−28.895	−2.0689	5.1499	4.2779
Φ	0.5000	0.5000	0.00119	0.00174
$\Psi*10^{7}$	23.126	1.4603	−41.853	−36.346
σ_{zx}	0.8662	0.0336	0.4837	0.4690
σ_{zy}	−0.8657	−0.0336	−0.2681	−0.2586
σ_{zz}	−0.4489	−0.0116	0.0421	0.0383
D_z*10^{10}	−137.32	−4.7884	−0.02848	−0.00212
B_z*10^{8}	−0.0801	0.0041	0.9956	1.5353
σ_{xx}	−5.1013	0.3230	−0.7688	−0.8069
σ_{yy}	−5.1014	0.3230	−1.0300	−1.0393
σ_{xy}	6.9426	0.1495	−0.5443	−0.5387
D_x*10^{12}	−23328.0	−759.32	−44.720	−8.7010
D_y*10^{12}	21726.0	694.78	22.533	2.2195
B_x*10^{8}	0.71429	0.0333	−1.4724	−2.5332
B_y*10^{8}	−0.6653	−0.0304	0.5817	2.0529

loading and localized uniformly distributed line loading are tabulated in Table 2. It is observed that the potential loading gives in general more values as compared to line loading in case of B/F/B plate. However, the trend is reversed in the case of F/B/F plate. It is interesting to note that the B/F/B plate under potential loading always shows critical values except B in which F/B/F plate shows critical values under line loading.

3.1.2. Example-2

The second example is a two-layered plate with piezoelectric $BaTiO_3$ is in the bottom layer and the magnetostrictive $CoFe_2O_4$ is in the top layer. Both the layers are assumed to have equal thickness. Starting from the top, this two-layered plate is named as F/B plate. The analysis is done with different a/h ratios under all edges simply supported (SSSS) as well as with two opposite edges simply supported and other two clamped (CSCS). A bi-sinusoidal external load with maximum value of $1\,N/m^2$ at the centre and zero values at edges has been applied at the top surface of the plate as shown in the Fig. 8 ($a = b = 0.8$ mm). In Figs. 9–13, the variations of Φ, σ_{xy}, D_x, σ_{zx}, and w across the thickness under bi-sinusoidal loading with 4×4 mesh size are plotted. In Fig. 9, it can be seen that for a plate having a/h ratio 2, slope of electric potential is positive at the bottom layer and is negative at the top layer. But as the value of a/h ratio increases, the slope of electric potential at the top layer is changing from negative to positive. The pattern of variation is found to be same on both the boundary conditions. Fig. 10 shows that as a/h ratio increases, variation of in-plane shear stress is having almost similar nature. Fig. 11 shows that the electric displacement varies drastically across the $BaTiO_3$ layer and its value is zero in $CoFe_2O_4$ layer. The values of electric displacement are found to be decreasing with increase in the rigidity of the support and the pattern of variation is found to be the same for all a/h ratios. In Fig. 12, transverse shear stress shows a parabolic variation across the thickness of the plate.

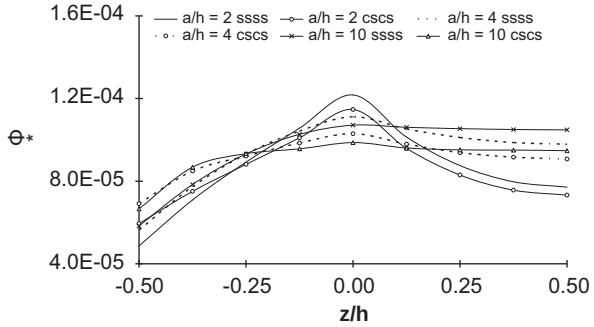

Fig. 9. Variation of $\mathbf{\Phi}$ across the thickness under bi-sinusoidal loading for F/B plate.

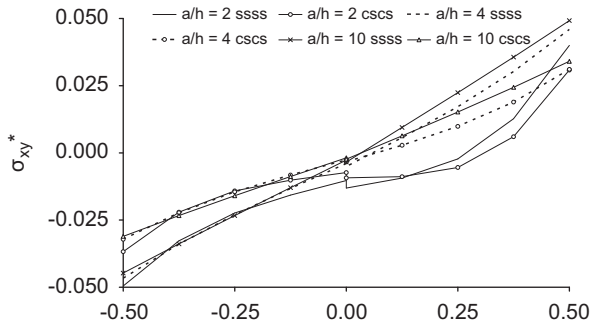

Fig. 10. Variation of σ_{xy} across the thickness under bi-sinusoidal loading for F/B plate.

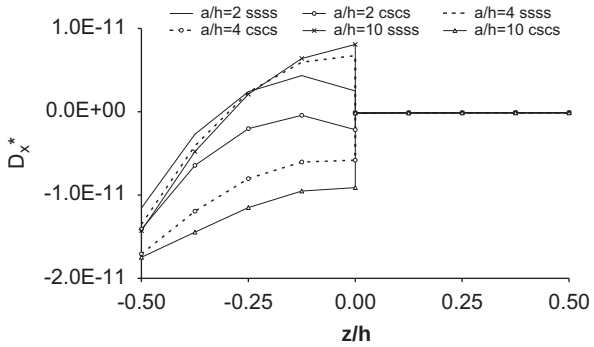

Fig. 11. Variation of D_x across the thickness under bi-sinusoidal loading for F/B plate.

Its maximum value is found to be increasing with increase in a/h ratio for all edges simply supported case and decreases with increase in a/h ratio for the case with two opposite edges clamped and the other two simply supported. It can be seen from Fig. 13 that the value of w is constant for a/h ratio greater than or equal to 4 and its value is slightly decreasing from top to bottom layer for plate having a/h ratio 2.

3.2. Dynamic analysis

3.2.1. Example-3

The problem of a simple supported square smart (p/0/90/0/p) laminate subjected to dynamic electric load in the form of applied voltage $V = V_0 \sin(\pi x/a) \sin(\pi y/b) \sin(\omega t)$ at the plate top surface as studied by Ray et al. [34] is considered in this example. The thickness of each surface bonded piezoelectric (PVDF) layer is 0.1 mm

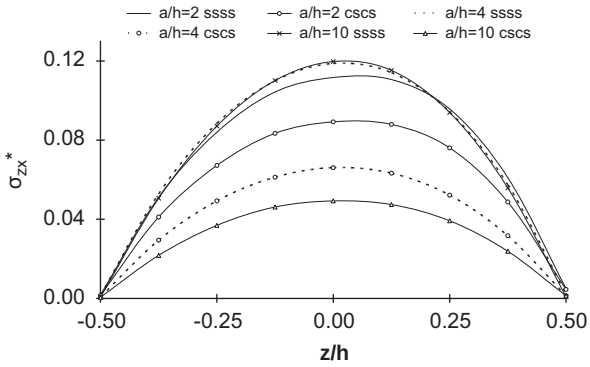

Fig. 12. Variation of σ_{zx} across the thickness under bi-sinusoidal loading for F/B plate.

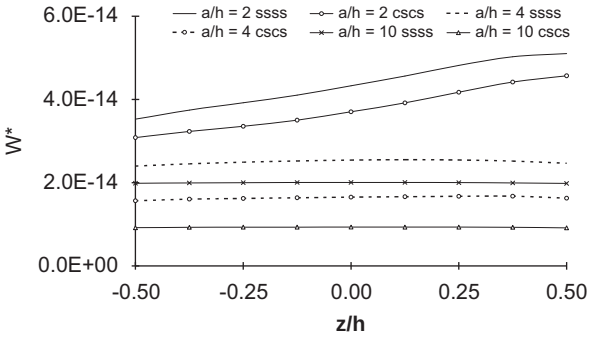

Fig. 13. Variation of w across the thickness under bi-sinusoidal loading for F/B plate.

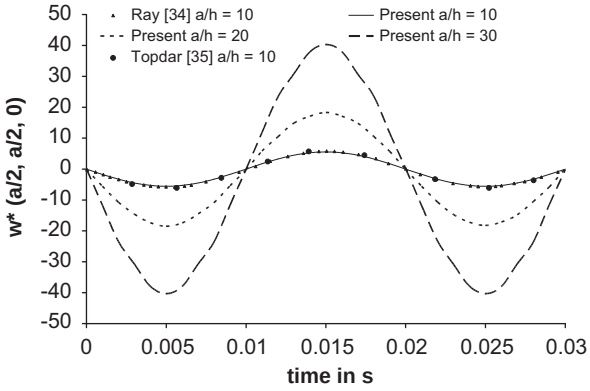

Fig. 14. Centre deflection of a smart plate (p/0/90/0/p) under applied potential.

and that of each layer in cross-ply (0/90/0) laminated core is 2.0 mm. The material properties and boundary conditions of the core layers and piezoelectric layers are taken as same as those given in Ray et al. [34]. In the present study, the plate is analysed with mesh size 4×4 based on the convergence, second-order variation for all degrees of freedom along thickness, taking $V_0 = 100\,\mathrm{V}$, $\omega = 100\pi\,\mathrm{rad/s}$, span to depth ratios $a/h = 10$, 20, and 30. The interfaces between the piezoelectric layers and core are grounded. The deflection values are normalized according to the following relationship: $(w^*, u^*) = E_2\ (w, u)/V_0\ e_{31}$. The normalized values of centre deflection (w^*) are plotted along with the exact solutions [34] and finite element solutions [35] in Fig. 14. It is observe that the results are in overall good agreement.

3.2.2. Example-4

In this example sandwich plates made of piezoelectric $BaTiO_3$ and magnetostrictive $CoFe_2O_4$ considered by Pan [3] is analysed with three different h/a ratios, i.e., $h/a = 0.3$, 0.1, and 0.01.The three layers have equal thickness of $h/3$ with a span of 1 mm. The analysis has been done under a bi-sinusoidal dynamic load ($p = p_0 \sin(\pi x/a)\sin(\pi y/b)\sin(\omega t)$) as shown in Fig. 15 and a uniformly distributed dynamic load ($p = p_0 \sin(\omega t)$). The value of ω is taken as 200π, which less than the natural frequency of the same plate presented in the article by Pan and Heyliger [7]. The results for convergence study for the first maximum value of deflection, w at centre ($x = 0.5$, $y = 0.5$, $z = 0.3$) for h/a ratio of 0.3 at time = 0.0025 s are tabulated in Table 3. Based on this convergence study, a (8×8) mesh for the quarter plate has been used for the computation of the results. The time history of deflection at centre of the plate obtained in the present analysis for a B/F/B plate is plotted in Figs. 16 and 17 and for F/B/F plate it is plotted in Figs. 18 and 19.The central deflection of both F/B/F and B/F/B plates shows similar pattern of variation for a/h ratios considered. But the curves are found to be smooth for plates having a/h ratio less than or equal to 10. It is observed that the deflection is more in general in case of uniformly distributed loading as compared to bi-sinusoidal loading for both the stacking sequences considered.

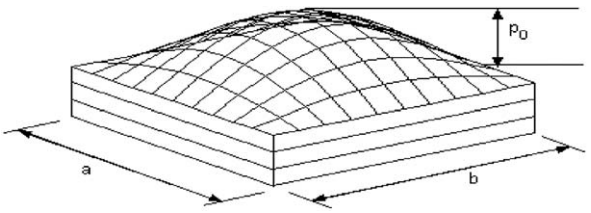

Fig. 15. Three layered plate subjected to bi-sinusoidal loading.

Table 3
Convergence study for w at centre ($x = 0.5$, $y = 0.5$, $z = 0.3$) of the plate ($a/h = 0.3$) at $t = 0.0025$ s.

No. of elements	w	Difference
16	1.226×10^{-11}	
36	1.249×10^{-11}	1.226–1.249 = −0.024
64	1.257×10^{-11}	1.249–1.257 = −0.007
100	1.260×10^{-11}	1.257–1.260 = −0.003
144	1.261×10^{-11}	1.260–1.261 = −0.001
196	1.262×10^{-11}	1.261–1.262 = −0.001

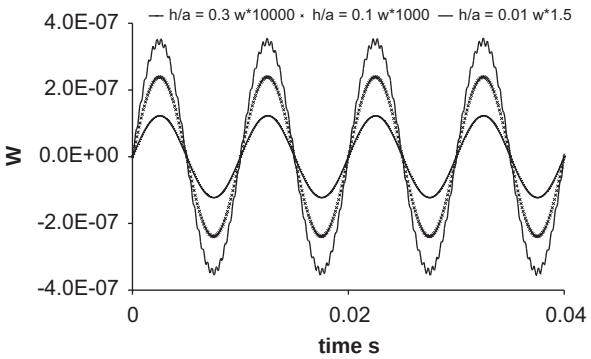

Fig. 16. Variation of w at centre for B/F/B plate under bi-sinusoidal loading.

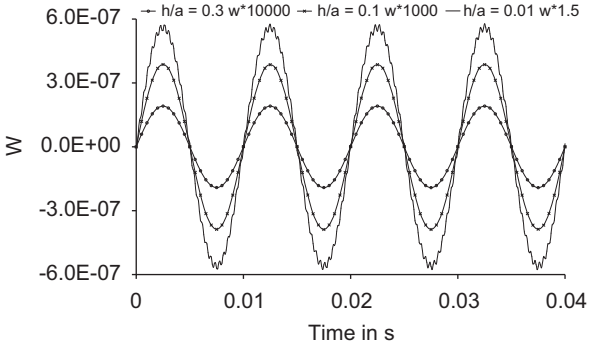

Fig. 17. Variation of w at centre for B/F/B plate under uniformly distributed loading.

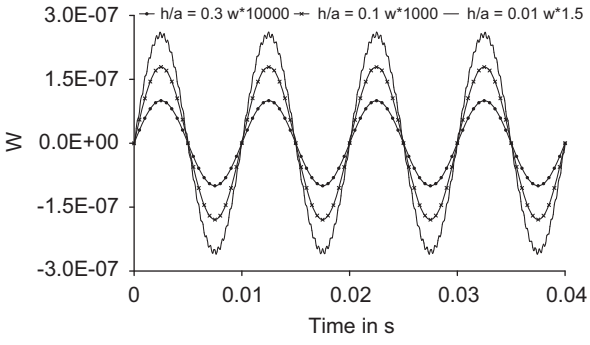

Fig. 18. Variation of w at centre for F/B/F plate under bi-sinusoidal loading.

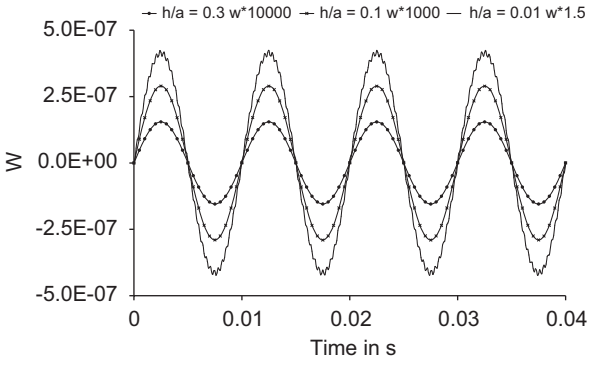

Fig. 19. Variation of w at centre for F/B/F plate under uniformly distributed loading.

3.2.3. Example-5

In this example, the behaviour of a square magneto-electro-elastic laminate under mechanical and magnetic loading has been studied for different span to depth ratios (10 and 100). The plate has four magnetic ($CoFe_2O_4$)/piezoelectric ($BaTiO_3$) layers each having thickness of 0.025 mm and two composite layers each having thickness of 0.1 mm. The material properties of the composite layers considered are given below

$$c_{11} = 134.9\,\text{GPa}, \quad c_{22} = 14.35\,\text{GPa}, \quad c_{33} = 14.35\,\text{GPa}, \quad c_{12} = 5.156\,\text{GPa}, \quad c_{13} = 5.156\,\text{GPa},$$
$$c_{23} = 7.133\,\text{GPa}, \quad c_{44} = 3.606\,\text{GPa}, \quad c_{55} = 5.654\,\text{GPa}, \quad c_{66} = 5.654\,\text{GPa}, \quad k_{11}/k_0 = 3.5,$$
$$k_{22}/k_0 = 3.0, \quad k_{33}/k_0 = 3.0, \quad k_0 = 8.85 \times 10^{-12}\,\text{C}^2/\text{Nm}^2$$

Both the loadings (mechanical and magnetic) considered have sinusoidal variation in x and y directions with peak value of $1.0\,N/m^2$ at the centre of the plate and zero values at the boundaries. The results for this case have also been computed with a (8×8) mesh size for a quarter of the plate with second-order variation for degrees of freedom along thickness (Table 3). However, the mesh size (4×4) also gives satisfactory results with first-order variation of degrees of freedom. The electric and magnetic potential at the bottom of the plate is taken as zero. Table 4 presents the transverse deflection, w at centre $(x = 0.5,\ y = 0.5)$ of the simply supported plate subjected to potential and line loading as defined earlier with z/h ratios for the two stacking sequences namely F/F/0/90/F/F and F/B/0/90/B/F having $a/h = 10$ and 100. It is observed that the deflection decreases as a/h ratio increases for the plate subjected to potential loading. However, the trend is reversed for the plate subjected to line loading. It is also observed that the deflection decreases in case of potential loading and increases in case of line loading when the stacking sequence changes from F/F/0/90/F/F to F/B/0/90/B/F for both the a/h ratios considered. It is interesting to note that there is definite significant first and second-order variation of the deflection across thickness direction for moderately thick plate $(a/h = 10)$ in particular stacking sequence F/F/0/90/F/F. However, these variations are very small for other stacking sequence.

Table 4
Results for simply supported plate for applied potential and line loading.

z/h	Deflection at the centre of the plate (w)							
	Magnetic load				Load			
	F/F/0/90/F/F		F/B/0/90/B/F		F/F/0/90/F/F		F/B/0/90/B/F	
	$a/h = 10$	$a/h = 100$	$a/h = 10$	$a/h = 100$	$a/h = 10$	$a/h = 100$	$a/h = 10$	$a/h = 100$
−0.5	−2.38E−09	−1.85E−09	−1.60E−09	−5.42E−10	9.80E−11	6.71E−07	1.03E−10	7.29E−07
−0.45833	−2.36E−09	−1.85E−09	−1.58E−09	−5.42E−10	9.82E−11	6.71E−07	1.04E−10	7.29E−07
−0.41667	−2.34E−09	−1.85E−09	−1.56E−09	−5.42E−10	9.83E−11	6.71E−07	1.04E−10	7.29E−07
−0.375	−2.31E−09	−1.85E−09	−1.56E−09	−5.42E−10	9.85E−11	6.71E−07	1.04E−10	7.29E−07
−0.33333	−2.29E−09	−1.85E−09	−1.56E−09	−5.42E−10	9.86E−11	6.71E−07	1.04E−10	7.29E−07
−0.16667	−2.32E−09	−1.85E−09	−1.57E−09	−5.42E−10	9.89E−11	6.71E−07	1.04E−10	7.29E−07
−1.5E−15	−2.35E−09	−1.85E−09	−1.58E−09	−5.42E−10	9.91E−11	6.71E−07	1.04E−10	7.29E−07
0.166667	−2.37E−09	−1.85E−09	−1.59E−09	−5.42E−10	9.92E−11	6.71E−07	1.05E−10	7.29E−07
0.333333	−2.35E−09	−1.85E−09	−1.59E−09	−5.42E−10	9.93E−11	6.71E−07	1.05E−10	7.29E−07
0.375	−2.39E−09	−1.85E−09	−1.59E−09	−5.42E−10	9.92E−11	6.71E−07	1.04E−10	7.29E−07
0.416667	−2.38E−09	−1.85E−09	−1.59E−09	−5.42E−10	9.91E−11	6.71E−07	1.04E−10	7.29E−07
0.458333	−2.24E−09	−1.85E−09	−1.56E−09	−5.42E−10	9.89E−11	6.71E−07	1.04E−10	7.29E−07
0.5	−2.23E−09	−1.85E−09	−1.53E−09	−5.42E−10	9.87E−11	6.71E−07	1.04E−10	7.29E−07

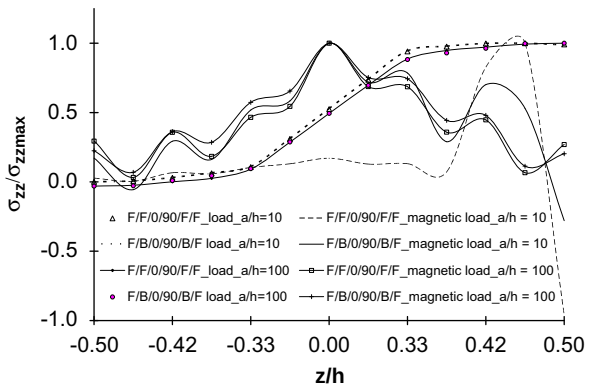

Fig. 20. Variation of σ^*_{zz} at centre of the simply supported plate.

The variations of normalized transverse normal stress across the thickness of the plate are shown in Fig. 20. It can be seen that for both the plates, variation of normalized transverse stress shows similar variation under mechanical loading for plates having a/h ratio 10 and 100. But, it varies considerably in each layer under magnetic loading with a similar pattern of variation for plates having a/h ratio 10 and 100.

4. Conclusions

In this paper an extension of the RMVT for the static and dynamic analysis of magneto-electro-elastic plate problem is presented and implemented. A finite element for the proposed RMVT model is also presented. Gaussian selective reduced integration scheme is adopted for terms related to transverse shear energy to avoid shear locking. In the present formulation, the C_z^0 requirements are satisfied a priori and no post processing operations are required to calculate transverse stresses. The static and transient forced vibration analysis of magneto-electro-elastic plates with different boundary conditions and span to depth ratios are solved with the code written in C-language. The both static and dynamic results are compared with those available in the literature and are found to be in good agreement. The results demonstrate the importance of the RMVT model for the problem.

Appendix A

$$\mathbf{K}_{uu}^{k\tau sij} = \int_{\Omega} \mathbf{D}_p^{\mathrm{T}}(N_i\mathbf{I})\bar{\mathbf{c}}_{pp}^{k\tau s}\mathbf{E}_{\tau s}\mathbf{D}_p(N_j\mathbf{I})\,\mathrm{d}\Omega; \quad \mathbf{K}_{\sigma\sigma}^{k\tau sij} = \int_{\Omega}(-N_i\bar{\mathbf{c}}_{nn}^{k\tau s}\mathbf{E}_{\tau s}N_j)\,\mathrm{d}\Omega \tag{A.1}$$

$$\mathbf{K}_{u\sigma}^{k\tau sij} = \int_{\Omega}(\mathbf{D}_p^{T}(N_i\mathbf{I})\bar{\mathbf{c}}_{pn}^{k\tau s}\mathbf{E}_{\tau s}N_j + \mathbf{D}_{n\Omega}^{T}(N_i\mathbf{I})E_{\tau s}N_j + E_{\tau_{,z}s}N_iN_j\mathbf{I})\,\mathrm{d}\Omega \tag{A.2}$$

$$\mathbf{K}_{\sigma u}^{k\tau sij} = \int_{\Omega}(N_iE_{\tau s}\mathbf{D}_{n\Omega}(N_j\mathbf{I}) + E_{\tau s_{,z}}N_iN_j\mathbf{I} - N_i\bar{\mathbf{c}}_{np}^{k\tau s}\mathbf{E}_{\tau s}\mathbf{D}_p(N_j\mathbf{I}))\,\mathrm{d}\Omega \tag{A.3}$$

$$\mathbf{K}_{ue}^{k\tau sij} = \int_{\Omega}(\mathbf{D}_p^{\mathrm{T}}(N_i\mathbf{I})\bar{\mathbf{c}}_{se}^{k\tau s}\mathbf{E}_{\tau s}N_j + \mathbf{D}_p^{\mathrm{T}}(N_i\mathbf{I})\bar{\mathbf{c}}_{se}^{k\tau s}\mathbf{E}_{\tau s_{,z}}I^*N_j)\,\mathrm{d}\Omega \tag{A.4}$$

$$\mathbf{K}_{\sigma e}^{k\tau sij} = -\int_{\Omega}(N_i\bar{\mathbf{c}}_{de}^{k\tau s}\mathbf{E}_{\tau s}\mathbf{D}_{ep}N_j + N_i\bar{\mathbf{c}}_{de}^{k\tau s}\mathbf{E}_{\tau s_{,z}}I^*N_j)\,\mathrm{d}\Omega \tag{A.5}$$

$$\mathbf{K}_{\sigma q}^{k\tau sij} = -\int_{\Omega}(N_i\bar{\mathbf{c}}_{dq}^{k\tau s}\mathbf{E}_{\tau s}\mathbf{D}_{ep}N_j + N_i\bar{\mathbf{c}}_{dq}^{k\tau s}\mathbf{E}_{\tau s_{,z}}I^*N_j)\,\mathrm{d}\Omega \tag{A.6}$$

$$\mathbf{K}_{uq}^{k\tau sij} = \int_{\Omega}(\mathbf{D}_p^{\mathrm{T}}N_i\bar{\mathbf{c}}_{sq}^{k\tau s}\mathbf{E}_{\tau s}\mathbf{D}_{ep}N_j + \mathbf{D}_p^{\mathrm{T}}N_i\bar{\mathbf{c}}_{sq}^{k\tau s}\mathbf{E}_{\tau s_{,z}}I^*N_j)\,\mathrm{d}\Omega \tag{A.7}$$

$$\mathbf{K}_{qu}^{k\tau sij} = -\int_{\Omega}(\mathbf{D}_{ep}^{\mathrm{T}}N_i\bar{\mathbf{c}}_{qd}^{k\tau s}\mathbf{E}_{\tau s}\mathbf{D}_pN_j + I^{*\mathrm{T}}N_i\bar{\mathbf{c}}_{qd}^{k\tau s}\mathbf{E}_{\tau_{,z}s}\mathbf{D}_pN_j)\,\mathrm{d}\Omega \tag{A.8}$$

$$\mathbf{K}_{eu}^{k\tau sij} = -\int_{\Omega}(\mathbf{D}_{ep}^{\mathrm{T}}N_i\bar{\mathbf{c}}_{ed}^{k\tau s}\mathbf{E}_{\tau s}\mathbf{D}_pN_j + I^{*\mathrm{T}}N_i\bar{\mathbf{c}}_{ed}^{k\tau s}\mathbf{E}_{\tau_{,z}s}\mathbf{D}_pN_j)\,\mathrm{d}\Omega \tag{A.9}$$

$$\mathbf{K}_{q\sigma}^{k\tau sij} = -\int_{\Omega}(\mathbf{D}_{ep}^{\mathrm{T}}N_i\bar{\mathbf{c}}_{qs}^{k\tau s}\mathbf{E}_{\tau s}N_j + I^{*\mathrm{T}}N_i\bar{\mathbf{c}}_{qs}^{k\tau s}\mathbf{E}_{\tau_{,z}s}N_j)\,\mathrm{d}\Omega \tag{A.10}$$

$$\mathbf{K}_{eq}^{k\tau sij} = -\int_{\Omega}\begin{pmatrix}\mathbf{D}_{ep}^{\mathrm{T}}N_i\bar{\mathbf{c}}_{eq}^{k\tau s}\mathbf{E}_{\tau s}\mathbf{D}_{ep}N_j + \mathbf{D}_{ep}^{\mathrm{T}}N_i\bar{\mathbf{c}}_{eq}^{k\tau s}\mathbf{E}_{\tau s_{,z}}I^*N_j + \\ I^{*\mathrm{T}}N_i\bar{\mathbf{c}}_{eq}^{k\tau s}\mathbf{E}_{\tau_{,z}s_{,z}}I^*N_j + I^{*\mathrm{T}}N_i\bar{\mathbf{c}}_{eq}^{k\tau s}\mathbf{E}_{\tau_{,z}s}\mathbf{D}_{ep}N_j\end{pmatrix}\mathrm{d}\Omega \tag{A.11}$$

$$\mathbf{K}_{qe}^{k\tau sij} = -\int_{\Omega}\begin{pmatrix}\mathbf{D}_{ep}^{\mathrm{T}}N_i\bar{\mathbf{c}}_{qe}^{k\tau s}\mathbf{E}_{\tau s}\mathbf{D}_{ep}N_j + \mathbf{D}_{ep}^{\mathrm{T}}N_i\bar{\mathbf{c}}_{qe}^{k\tau s}\mathbf{E}_{\tau s_z}I^*N_j + \\ I^{*\mathrm{T}}N_i\bar{\mathbf{c}}_{qe}^{k\tau s}\mathbf{E}_{\tau_z s_z}I^*N_j + I^{*\mathrm{T}}N_i\bar{\mathbf{c}}_{qe}^{k\tau s}\mathbf{E}_{\tau_z s}\mathbf{D}_{ep}N_j\end{pmatrix}\mathrm{d}\Omega \tag{A.12}$$

$$\mathbf{K}_{ee}^{k\tau sij} = -\int_{\Omega}\begin{pmatrix}\mathbf{D}_{ep}^{\mathrm{T}}N_i\bar{\mathbf{c}}_{ee}^{k\tau s}\mathbf{E}_{\tau s}\mathbf{D}_{ep}N_j + \mathbf{D}_{ep}^{\mathrm{T}}N_i\bar{\mathbf{c}}_{ee}^{k\tau s}\mathbf{E}_{\tau s_z}I^*N_j + \\ I^{*\mathrm{T}}N_i\bar{\mathbf{c}}_{ee}^{k\tau s}\mathbf{E}_{\tau_z s_z}I^*N_j + I^{*\mathrm{T}}N_i\bar{\mathbf{c}}_{ee}^{k\tau s}\mathbf{E}_{\tau_z s}\mathbf{D}_{ep}N_j\end{pmatrix}\mathrm{d}\Omega \tag{A.13}$$

$$\mathbf{K}_{qq}^{k\tau sij} = -\int_{\Omega}\begin{pmatrix}\mathbf{D}_{ep}^{\mathrm{T}}N_i\bar{\mathbf{c}}_{qq}^{k\tau s}\mathbf{E}_{\tau s}\mathbf{D}_{ep}N_j + \mathbf{D}_{ep}^{\mathrm{T}}N_i\bar{\mathbf{c}}_{qq}^{k\tau s}\mathbf{E}_{\tau s_z}I^*N_j + \\ I^{*\mathrm{T}}N_i\bar{\mathbf{c}}_{qq}^{k\tau s}\mathbf{E}_{\tau_z s_z}I^*N_j + I^{*\mathrm{T}}N_i\bar{\mathbf{c}}_{qq}^{k\tau s}\mathbf{E}_{\tau_z s}\mathbf{D}_{ep}N_j\end{pmatrix}\mathrm{d}\Omega \tag{A.14}$$

$$(E_{\tau s}, E_{\tau s_z}, E_{\tau_z s}, E_{\tau_z s_z}) = \int_z (F_\tau F_s, F_\tau F_{s_z}, F_{\tau_z} F_s, F_{\tau_z} F_{s_z})\,\mathrm{d}z \tag{A.15}$$

$$I^{*\mathrm{T}} = [0 \;\; 0 \;\; -1] \tag{A.16}$$

References

[1] D.A. Saravanos, P.R. Heyliger, D.A. Hopkins, Layerwise mechanics and finite element for the dynamic analysis of piezoelectric composite plates, *International Journal of Solids and Structures* 34 (1997) 359–378.

[2] D.A. Saravanos, P.R. Heyliger, Mechanics and computational models for laminated piezoelectric beams plates and shells, *Applied Mechanics Review* 52 (1999) 305–320.

[3] E. Pan, Exact solution for simply supported and multilayered magneto-electro-elastic plates, *Transactions of the ASME* 68 (2001) 608–618.

[4] Q. Guan, S.R. He, Three-dimensional analysis of piezoelectric/piezomagnetic elastic media, *Composite Structures* 72 (2006) 419–428.

[5] E. Pan, P.R. Heyliger, Exact solutions for magneto-electro-elastic laminates in cylindrical bending, *International Journal of Solids and Structures* 40 (2003) 6859–6876.

[6] E. Pan, F. Han, Exact solution for functionally graded and layered magneto-electro-elastic plates, *International Journal of Engineering Science* 43 (2005) 321–339.

[7] E. Pan, P.R. Heyliger, Free vibrations of simply supported and multilayered magneto-electro-elastic plates, *Journal of Sound and Vibration* 252 (3) (2002) 429–442.

[8] W.Q. Chen, K.Y. Leeb, H.J. Ding, On free vibration of non-homogeneous transversely isotropic magneto-electro-elastic plates, *Journal of Sound and Vibration* 279 (2005) 237–251.

[9] J. Wang, L. Chen, S. Fang, State vector approach to analysis of multilayered magneto-electro-elastic plates, *International Journal of Solids and Structures* 40 (2003) 1669–1680.

[10] J. Chen, H. Chen, E. Pan, P.R. Heyliger, Modal analysis of magneto-electro-elastic plates using the state-vector approach, *Journal of Sound and Vibration* 304 (2007) 722–734.

[11] W.Q. Chen, K.Y. Lee, Alternative state space formulations for magnetoelectric thermoelasticity with transverse isotropy and the application to bending analysis of nonhomogeneous plates, *International Journal of Solids and Structures* 40 (2003) 5689–5705.

[12] J. Aimin, W. Guoquan, Q. Honglin, The boundary contour method for magneto-electro-elastic media with quadratic boundary elements, *International Journal of Solids and Structures* 44 (18–19) (2007) 6220–6231.

[13] R.K. Bhangale, N. Ganesan, Static analysis of simply supported functionally graded and layered magnetoelectroelastic plates, *International Journal of Solids and Structures* 43 (2006) 3230–3253.

[14] R.K. Bhangale, N. Ganesan, Free vibration of simply supported functionally graded and layered magneto-electro-elastic plates by finite element method, *Journal of Sound and Vibration* 294 (2006) 1016–1038.

[15] Z. Chen, S. Yu, L. Meng, Y. Lin, Effective properties of layered magneto-electro-elastic composites, *Composite Structures* 57 (2002) 177–182.

[16] W.Q. Chen, K.Y. Lee, H.J. Ding, General solution for transversely isotropic magneto-electro-thermo-elasticity and the potential theory method, *International Journal of Engineering Science* 42 (2004) 1361–1379.

[17] P.F. Hou, Y.T.A. Leung, H.J. Ding, The elliptical Hertzian contact of transversely isotropic magneto-electro-elastic bodies, *International Journal of Solids and Structures* 40 (2003) 2833–2850.

[18] A.R. Annigeri, N. Ganesan, S. Swarnamani, Free vibration behaviour of multiphase and layered magneto-electro-elastic beam, *Journal of Sound and Vibration* 299 (2007) 44–63.

[19] F. Ramirez, P.R. Heyliger, E. Pan, Free vibration response of two-dimensional magneto-electro-elastic laminated plates, *Journal of Sound and Vibration* 292 (2006) 626–644.

[20] A. Toledano, H. Murakami, A high-order laminated plate theory with improved in-plane response, *International Journal of Solids and Structures* 23 (1987) 111–131.
[21] E. Carrera, Evaluation of layer-wise mixed theories for laminated plate analysis, *AIAA Journal* 36 (1998) 830–839.
[22] E. Carrera, Theories and finite elements for multilayered plates and shells: a unified compact formulation with numerical assessment and bench marking, *Archives of Computational Methods in Engineering* 10 (2003) 215–297.
[23] E. Carrera, An assessment of mixed and classical theories on global and local response of multilayered orthotropic plates, *Composite Structures* 50 (2000) 183–198.
[24] E. Carrera, Developments, ideas and evaluations based upon Reissner's mixed variational theorem in the modeling of multilayered plates and shells, *Applied Mechanics Review* 54 (2001) 301–329.
[25] E. Carrera, M. Boscolo, A. Robaldo, Hierarchic multilayered plate elements for coupled multifield problems of piezoelectric adaptive structures: formulation and numerical assessment, *Archives of Computational Methods in Engineering* 14 (2007) 383–430.
[26] E. Carrera, M. Boscolo, Classical and mixed elements for static and dynamic analysis of piezoelectric plates, *International Journal for Numerical Methods in Engineering* 70 (2007) 253–291.
[27] E. Carrera, S. Brischetto, P. Nali, Variational statements and computational models for multifield problems and multilayered structures, *Mechanics of Advanced Materials and Structures* 15 (2008) 182–198.
[28] A. Benjeddou, O. Andrianarison, A piezoelectric mixed variational theorem for smart multilayered composites, *Mechanics of Advanced Materials and Structures* 12 (2005) 1–12.
[29] M.D. Ottavio, B. Kroplin, An extension of Reissner mixed variational theorem to piezoelectric laminates, *Mechanics of Advanced Materials and Structures* 13 (2006) 139–150.
[30] J.S. Yang, R.C. Batra, Mixed variational principles in nonlinear electroelasticity, *International Journal of Non-Linear Mechanics* 30 (5) (1995) 719–725.
[31] R.G. Lage, C.M.M. Soares, C.A.M. Soares, J.N. Reddy, Layer-wise partial mixed finite element analysis of magneto-electro-elastic plates, *Computers and Structures* 82 (2004) 1293–1301.
[32] E. Carrera, L. Demasi, Classical and advanced multilayered plate elements based upon PVD and RMVT, part 1, derivation of finite element matrices, *International Journal of Numerical Methods in Engineering* 55 (2002) 191–231.
[33] K.J. Bathe, E.L. Wilson, *Numerical Methods in Finite Element Analysis*, Prentice-Hall, Englewood Cliffs, NJ, 1976.
[34] M.C. Ray, R. Bhattacharya, B. Samanta, Exact solutions for dynamic analysis of composite plates with distributed piezoelectric layers, *Computers and Structures* 66 (6) (1998) 737–743.
[35] P. Topdar, A.H. Sheikh, N. Dhang, Response and control of smart laminates using a refined hybrid plate model, *AIAA Journal* 44 (11) (2006) 2636–2644.